A POWER-BALANCED DYNAMIC MODEL OF FERROMAGNETIC COILS

Judy Najnudel and Rémy Müller

S3AM Team, STMS laboratory (UMR 9912)
IRCAM-CNRS-SU
Paris, France
judy.najnudel@ircam.fr
remy.muller@ircam.fr

*Thomas Hélie and David Roze**

CNRS
S3AM Team, STMS laboratory (UMR 9912)
IRCAM-CNRS-SU
Paris, France
thomas.helie@ircam.fr
david.roze@ircam.fr

ABSTRACT

This paper proposes a new macroscopic physical model of ferromagnetic coils used in audio circuits. To account for realistic saturation and hysteretic phenomena, this model combines statistical physics results, measurement-driven refinements and port-Hamiltonian formulations that guarantee passivity, thermodynamic consistency and composability according to both electric and thermal ports. As an illustration, the model is used to simulate a passive high-pass filter. Different types of audio inputs are considered and simulations are compared to measurements.

1. INTRODUCTION

Ferromagnetism is frequent in analog audio: it is involved in transducers (dynamic microphones, loudspeakers), tape recorders, coils and transformers. As major non-linearities arise from ferromagnetic components (saturation, hysteresis), the need of refined models is critical to accurately simulate behaviors in circuits.

Since the 1980s, a large body of empirical models have been proposed, among them the Jiles-Atherton model [1], the Gyrator-Capacitor model [2, 3], or the Preisach model [4]. But very few have a strong physical meaning [5] and those retaining some energetic interpretation [6] either lose major phenomenological properties or are heavy to implement [7]. As a consequence, preserving the model passivity (no artificial hidden sources of energy) comes with a price — computation time.

In this paper, we propose a new nonlinear model of ferromagnetic coil that is physically-based, passive, modular (allowing electric and thermal connections) and with a reduced complexity (few state variables and parameters). As it is built on statistical physics results on magnets, it is thermodynamically consistent. It also inherits macroscopic characteristics (hysteresis and its conditioned activation) from underlying microscopic phenomena (metastability and phase transition). This lumped-element model is used to simulate a passive high-pass filter. The circuit modeling relies on Port-Hamiltonian Systems [8, 9] (PHS) that structurally fulfill the power balance. Simulations are based on numerical methods [10] that preserve this guarantee in the discrete-time domain.

The paper is structured as follows: Section 2 first presents some short recalls on PHS. Section 3 develops a primary model derived from statistical physics. This model exhibits saturation and hysteresis but does not take into account some other phenomena, such as non-homogeneities, thermal fluctuations and eddy currents. Section 4 refines the primary model with a polynomial interpolation based on measurements of a Fasel inductor. In section 5, the final nonlinear model is implemented to simulate a passive high-pass filter.

* The authors acknowledge the support of the ANR-DFG (French- German) project INFIDHEM ANR-16-CE92-0028.

2. REVIEW OF PORT-HAMILTONIAN SYSTEMS

The following modeling relies on Port-Hamiltonian systems [11, 9], under a differential-algebraic formulation [10]. A dynamical system is represented as a network of: (i) storage components of state $\boldsymbol{x}$ and energy $E(\boldsymbol{x})$, (ii) dissipative components described by an efforts law $\boldsymbol{w} \mapsto z(\boldsymbol{w})$ that dissipates the power $P_{\text{diss}} = z(\boldsymbol{w})^\intercal \boldsymbol{w} \geq 0$ for all flows $\boldsymbol{w}$, and (iii) connection ports conveying the *outgoing* power $P_{\text{ext}} = \boldsymbol{u}^\intercal \boldsymbol{y}$ for inputs $\boldsymbol{u}$ and outputs $\boldsymbol{y}$. The flows $\boldsymbol{f}$ and efforts $\boldsymbol{e}$ of all the components are coupled through a skew-symmetric interconnection matrix $\boldsymbol{J} = -\boldsymbol{J}^\intercal$:

$$\underbrace{\begin{bmatrix} \dot{\boldsymbol{x}} \\ \boldsymbol{w} \\ \boldsymbol{y} \end{bmatrix}}_{\boldsymbol{f}} = \boldsymbol{J} \underbrace{\begin{bmatrix} \nabla E(\boldsymbol{x}) \\ z(\boldsymbol{w}) \\ \boldsymbol{u} \end{bmatrix}}_{\boldsymbol{e}}. \tag{1}$$

Such systems satisfy the power balance $P_{\text{stored}} + P_{\text{diss}} + P_{\text{ext}} = 0$ where $P_{\text{stored}} = \nabla E(\boldsymbol{x})^\intercal \dot{\boldsymbol{x}}$ denotes the stored power. Indeed, $P_{\text{stored}} + P_{\text{diss}} + P_{\text{ext}} = \boldsymbol{e}^\intercal \boldsymbol{f} = \boldsymbol{e}^\intercal \boldsymbol{J} \boldsymbol{e}$ is zero since $\boldsymbol{e}^\intercal \boldsymbol{J} \boldsymbol{e} = (\boldsymbol{e}^\intercal \boldsymbol{J} \boldsymbol{e})^\intercal = -(\boldsymbol{e}^\intercal \boldsymbol{J} \boldsymbol{e})$ due to the skew-symmetry of $\boldsymbol{J}$.

All models herein will be formulated as (1).

3. PRIOR THEORETICAL MODEL

3.1. Macroscopic model of a ferromagnetic core

This section presents a bi-stable core model rooted in the *mean field Ising model* [12, 13, 14, 15, 16]. Using statistical physics, Ising derives a macroscopic scalar state (the core magnetization) from a microscopic representation of the core (a set of normalized atomic magnetic moments, which can be either up or down), at a given temperature T. For simplicity, additional assumptions are: a homogeneous, isochoric (constant volume V) and closed (constant number of atoms N) ferromagnetic crystal with one (local) magnetization axis and periodic boundaries (typically, a toroidal geometry often found in audio circuits [17]). In this section, there is no external magnetic field (issue addressed in section 3.2).

3.1.1. *Macroscopic quantities and laws*

Following [18] with our assumptions, the core internal energy is

$$E = N\alpha\left(\frac{1}{2}m^2 - m\,\tanh\left(\frac{m}{\theta}\right)\right), \tag{2}$$

where parameter α ($\approx 5\times10^{-21}$ J for transition metals) denotes the *exchange energy* between one moment and its nearest neighbours [19, 20, 21], and where variables m and θ are average intensive quantities (homogeneous over the body) that statistically characterize the core configuration at a macroscopic scale:

- $m \in [-1, 1]$ is the mean normalized magnetic moment: $m = \pm 1$ if all moments are aligned in the same direction, and $m = 0$ if no particular direction is favored;
- $\theta = T/T_c \in \mathbb{R}_+$ is the reduced temperature relative to the core Curie temperature T_c [22]: if $\theta < 1$, there are multiple equilibria m (ferromagnetism), and only $m = 0$ (disordered moments) otherwise (paramagnetism).

Note that the core parameters α and T_c are related through the Boltzmann constant $k_b = 1.38\times10^{-23}$J.K^{-1} as $\alpha = k_b\,T_c$.

A measure of the number of possible microscopic states (atomic moments) consistent with the core macroscopic configuration is given by the entropy [23], which is found to be

$$S = N\,k_b\,f\left(\frac{m}{\theta}\right)\ \text{with}\ f(\chi) = \ln(2\cosh\chi) - \chi\,\tanh\chi, \chi\in\mathbb{R}. \tag{3}$$

This statistical entropy coincides with the thermodynamic entropy for a core in internal thermodynamic equilibrium (possibly time-varying at macroscopic scale). This variable is extensive (proportional to N) and quantifies the macroscopic "order degree" of the core, on which phase transitions and hysteresis depend.

In addition to E and S, a third extensive variable is introduced, namely, the total magnetic flux of the core (of volume V)

$$B_V = B\,V, \tag{4}$$

where B is the magnetic flux density. For the core, B is related to the core magnetization $M = m\,M_s$ through $B = \mu_0\,M$ where μ_0 is the vacuum magnetic permeability and M_s is the saturation magnetization (see Table 1).

3.1.2. *Choice of state and energy function*

We choose to express the core energy E as a function of the state

$$\boldsymbol{x}_{\text{core}} = [B_V, S]^\intercal, \tag{5}$$

so that, in (1), the flow $\dot{\boldsymbol{x}}_{\text{core}}$ accounts for the time variation of extensive quantities (to balance with quantities external to the core, or *equilibrium-establishing*) and, concomitantly, the effort accounts for intensive quantities (shared with the exterior at the core interface, or *equilibrium-determining*). Choosing extensive energy variables over intensive co-energy variables stems from two arguments. The first one is physical: except for linear, mono-variate components, constitutive laws derived from the co-energy are not equal to those derived from the energy, and should be handled with care. The second is numerical: solving an ODE by integration instead of differentiation is generally preferable [11].

This function is derived from (2), in which m/θ and m are expressed with respect to S and B_V using (3-4) and noting that f is smooth, even on $\mathbb{R}$ and strictly monotonic[1] (so invertible) on $\mathbb{R}^+$. Its formula expressed w.r.t. (5) is given by (see Fig. 1),

$$\frac{E_{\text{core}}([B_V, S]^\intercal)}{E_0} = \frac{1}{2}\left(\frac{B_V}{B_{V_s}}\right)^2 - \left|\frac{B_V}{B_{V_s}}\right|\tanh\left(f^{-1}\left(\frac{S}{S_0}\right)\right), \tag{6}$$

with core constants $E_0 = N\alpha$, $S_0 = N\,k_b$ and $B_{V_s} = V\,\mu_0 M_s$. The energy gradient (effort) is

$$\nabla E_{\text{core}} = [H_{\text{core}}, T_{\text{core}}]^\intercal, \tag{7}$$

where, omitting variables in functions, the core internal magnetic field is

$$\frac{\partial E_{\text{core}}}{\partial B_V} = \frac{E_0}{B_{V_s}}\left(\frac{B_V}{B_{V_s}} - \text{sign}\,(B_V)\tanh\left(f^{-1}\left(\frac{S}{S_0}\right)\right)\right) := H_{\text{core}} \tag{8}$$

and the core temperature is

$$\frac{\partial E_{\text{core}}}{\partial S} = \frac{E_0}{S_0}\left|\frac{B_V}{B_{V_s}}\right| / f^{-1}\left(\frac{S}{S_0}\right) := T_{\text{core}}. \tag{9}$$

Fig. 1 shows that as S increases, the core goes from two ordered (aligned moments) meta-stable equilibrium states to one non-ordered (no alignment) stable equilibrium state: it exhibits a phase transition (from ferromagnetic to paramagnetic). Table 1 recaps the physical quantities involved and their units.

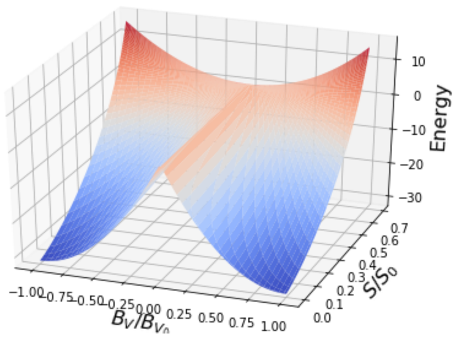

Figure 1: Core energy function with respect to B_V and S.

3.2. Connection to coil and external electrical ports

3.2.1. *Ideal coil model*

The coil is considered to be linear. Choosing B_V as its state variable, the coil energy is

$$E_{\text{coil}}(B_V) = \frac{B_V^2}{2\mu_0 V}, \tag{10}$$

and its derivative with respect to B_V is the coil magnetic field $H_{\text{coil}}(B_V) = B_V/(\mu_0 V)$.

[1] Indeed, $f'(\chi) = -\chi/\cosh^2\chi \le 0\ \forall\chi\in\mathbb{R}^+$.

Symbol	Quantity	S.I. units
N	atoms nb.	dimensionless
α	nearest neighbours exchange energy	kg.m^2.s.$^{-2}$
m	norm. magnetic moment	dimensionless
$\mathcal{M}$	magnetic moment	A.m^2
M	magnetization	A.m^{-1}
H	magnetic field	A.m^{-1}
B	magnetic flux density	kg.s^{-2}.A^{-1}
μ_0	vacuum magnetic permeability	kg.m.s^{-2}.A^{-2}
Φ	magnetic flux linkage	kg.m^2.s^{-2}.A^{-1}
n	coil turns nb.	dimensionless
k_b	Boltzmann constant	kg.m^2.s^{-2}.K^{-1}
T	temperature	K
S	entropy	kg.m^2.s^{-2}.K^{-1}
$V = Al$	volume = section x length	m^3
Label		
L	coupled core and coil	

Table 1: Physical quantities and labels.

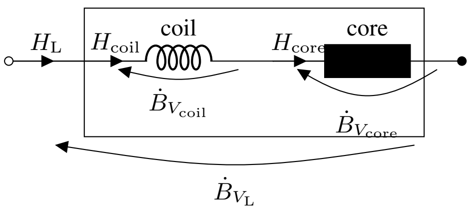

Figure 2: Coil and core connection.

3.2.2. *Coupled system*

To express the coupled system L as a PHS, one needs to determine the relations between the core and coil flows and efforts. Using the extensivity of the total magnetic moment $\mathcal{M}_\mathrm{L}$ [24], one gets

$$\mathcal{M}_\mathrm{L} = \mathcal{M}_\mathrm{core} + \mathcal{M}_\mathrm{coil} \Leftrightarrow B_{V_\mathrm{L}} = B_{V_\mathrm{core}} + B_{V_\mathrm{coil}}, \tag{11}$$

since $B_V = \mu_0 \mathcal{M}$. Differentiating Eq. (11) with respect to time, one obtains the relation between the flows:

$$\dot{B_{V_\mathrm{L}}} = \dot{B}_{V_\mathrm{core}} + \dot{B}_{V_\mathrm{coil}}. \tag{12}$$

Conversely, the coil and core share their efforts, namely,

$$H_\mathrm{L} = H_\mathrm{coil} = H_\mathrm{core}. \tag{13}$$

Fig. 2 represents the coupling as a series connection.
For any fixed entropy S and for all $\boldsymbol{x} = [B_{V_\mathrm{coil}}\ B_{V_\mathrm{core}}]^\intercal$, we introduce the function $E_\mathrm{S} : \boldsymbol{x} \mapsto E_\mathrm{core}(B_{V_\mathrm{core}}, S) + E_\mathrm{coil}(B_{V_\mathrm{coil}})$ (total energy of the system). With these notations, the core and coil coupling can be expressed as the constrained Dirac structure [25]

$$\begin{bmatrix} \dot{\boldsymbol{x}} \\ 0 \\ y \end{bmatrix} = \begin{bmatrix} \cdot & \boldsymbol{A} & \boldsymbol{B} \\ -\boldsymbol{A} & \cdot & \cdot \\ -\boldsymbol{B} & \cdot & \cdot \end{bmatrix} \begin{bmatrix} \frac{\partial E_\mathrm{S}}{\partial \boldsymbol{x}} \\ \lambda \\ u \end{bmatrix}, \tag{14}$$

with $\boldsymbol{A} = [1,\ -1]^\intercal$, $\boldsymbol{B} = [0,\ 1]^\intercal$, $\lambda = \dot{B}_{V_\mathrm{coil}}$, $u = \dot{B}_{V_\mathrm{L}}$ and $y = -H_\mathrm{L}$ (dots indicate zeros). This constrained Dirac structure can be reduced to (see also [25] for more details):

$$\begin{bmatrix} \dot{\boldsymbol{z}} \\ y \end{bmatrix} = \begin{bmatrix} \cdot & \boldsymbol{B_\mathrm{r}} \\ -\boldsymbol{B_\mathrm{r}} & \cdot \end{bmatrix} \begin{bmatrix} \frac{\partial E_\mathrm{L}}{\partial \boldsymbol{z}} \\ u \end{bmatrix}, \tag{15}$$

with $\tilde{\boldsymbol{A}}$ such as $\tilde{\boldsymbol{A}}^\intercal \boldsymbol{A} = 0$ to eliminate the constraint, $\boldsymbol{B_\mathrm{r}} = \tilde{\boldsymbol{A}}^\intercal \boldsymbol{B}$, $\boldsymbol{z} = \tilde{\boldsymbol{A}}^\intercal \boldsymbol{x}$, E_L the total energy with respect to $\boldsymbol{z}$.
Taking $\tilde{\boldsymbol{A}} = [1,\ 1]^\intercal$, this yields $\boldsymbol{B_\mathrm{r}} = 1$ and $\boldsymbol{z} = B_{V_\mathrm{coil}} + B_{V_\mathrm{core}}$. Therefore, for any given entropy S, the dynamics of the coupled system is that of an equivalent component of state $\boldsymbol{x}_\mathrm{L} = [B_{V_\mathrm{L}}, S]$, energy $E_\mathrm{L}(\boldsymbol{x}_\mathrm{L})$ and magnetic field $H_\mathrm{L} = \frac{\partial E_\mathrm{L}}{\partial B_{V_\mathrm{L}}}$. This equivalent component energy can be computed (see [26] for a detailed derivation) through the expression

$$\begin{aligned} E_\mathrm{L}(B_{V_\mathrm{L}}, S) = &\left(E_\mathrm{coil} \circ H_\mathrm{coil}^{-1} + E_\mathrm{core} \circ H_\mathrm{core}^{-1}\right) \\ &\circ \left(H_\mathrm{coil}^{-1} + H_\mathrm{core}^{-1}\right)^{-1} (B_{V_\mathrm{L}}, S), \end{aligned} \tag{16}$$

where the symbol $\circ$ stands for function composition. In practice, all mathematical functions in this expression can be defined as piecewise affine functions (computation of inverse efforts in particular becomes straightforward when analytical expressions are not available, as is the case here).

3.2.3. *Connection to external electrical ports*

Denoting n the number of turns, l the length of the coil, A its section, Φ the magnetic flux linkage, the magnetic field H_L is related to coil current i_L through

$$H_\mathrm{L} = \frac{n}{l} i_\mathrm{L}, \tag{17}$$

and the state B_{V_L} is related to the coil voltage v_L through

$$\dot{B}_{V_\mathrm{L}} = \frac{\dot{\Phi}}{nA} V = \frac{l}{n} v_\mathrm{L}. \tag{18}$$

In section 4.4, variables i_L and v_L will be related to external ports $\boldsymbol{u}$ and $\boldsymbol{y}$ of Eq. (1).

3.3. Thermodynamics

In this section (only), we assume that the ferromagnetic coil is put in a isothermal bath (i.e. the exterior is much larger than the coil size), so that the temperature of the system T_L is considered constant and equal to the exterior temperature T_ext during a change of state, supposedly below the Curie temperature. A convenient and classical way to study the energetic behavior of the ferromagnetic coil is to examine how, for all B_{V_L}, the energy $E_\mathrm{L}(B_{V_\mathrm{L}}, S)$ of the component subject to a constant magnetic field H_0, deviates from the energy $H_0\, B_{V_\mathrm{L}}$. The energy deviation of this conditioned component, called the Gibbs free energy [27], is defined by, for all B_{V_L}, S, and all constant-in-time H_0 as

$$G_{H_0}(B_{V_\mathrm{L}}, S) = E_\mathrm{L}(B_{V_\mathrm{L}}, S) - T_\mathrm{L} S - H_0\, B_{V_\mathrm{L}}. \tag{19}$$

For any given S, at $H_0 = 0$, two symmetric meta-stable equilibrium states corresponding to G_{H_0} minima with respect to B_{V_L} are available (Fig. 3a, red curve). For $H_0 \neq 0$, the symmetry is broken and a previously stable equilibrium state can be made unstable. We suppose now H_0 slowly controlled (so it is still considered constant during a change of state). When decreasing H_0

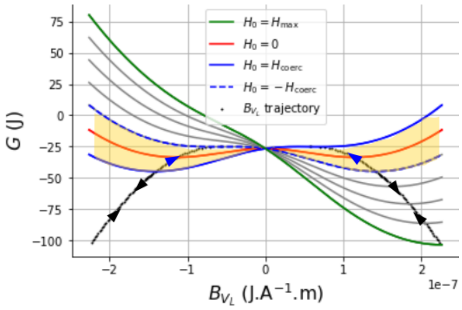

(a) Gibbs free energy G_{H_0} for H_0 decreasing from $H_{\max}$ (green curve) to H_{coerc} (solid blue curve), at constant temperature, and trajectory of B_{V_L} (black curve) for a complete cycle. In the yellow area, two local potential minima coexist but only one direction is possible for B_{V_L} to follow (blue arrows).

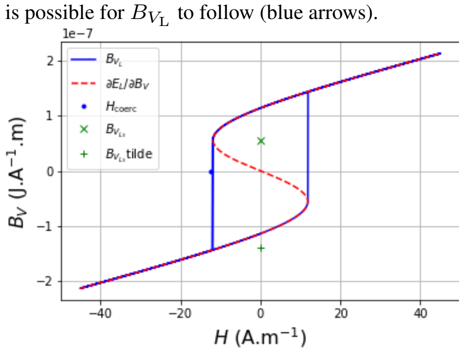

(b) Observed state B_{V_L} during a complete cycle, resulting in Barkhausen jumps (blue curve), and theoretical effort $\frac{\partial E_L}{\partial B_V}$ for B_V ranging from $\min(B_{V_L})$ to $\max(B_{V_L})$ (red curve). The area between the blue and red curves is the energy dissipated during a cycle.

Figure 3: Gibbs free energy G_{H_0} for decreasing values of magnetic field H_0 (3a), and observed state B_{V_L} during a complete cycle of magnetic field variations (3b).

from $H_{\max} \geq 0$ (Fig. 3a, green curve) to $-H_{\max}$, B_{V_L} starts from its initial equilibrium state and follows a trajectory solution of $\frac{\partial G_{H_0}}{\partial B_{V_L}} = 0$ (Fig. 3a, black curve), until the minimum degenerates into an inflection point at $H_0 = H_{\text{coerc}}$ (Fig. 3a, solid blue curve). Then, a Barkhausen jump occurs [27] so that B_{V_L} occupies the remaining stable equilibrium state (Fig. 3a, intersection of solid blue curve and left yellow area). Since E_L is even with respect to B_{V_L} for all S, $G_{H_0}(B_{V_L}, S) = G_{-H_0}(-B_{V_L}, S)$. Therefore, when increasing H_0 from $-H_{\max}$ to $H_{\max}$, the Barkhausen jump occurs at $-H_{\text{coerc}}$. Consequently, B_{V_L} follows a different path depending on whether H_0 decreases or increases (Fig. 3a, black curve and arrows), hence the hysteresis (Fig. 3b) between H_{coerc} and $-H_{\text{coerc}}$.
Thermodynamics laws show that the difference of energy before and after the jump is irreversibly dissipated as heat. Indeed, the first principle of thermodynamics states that the internal energy variation $\mathrm{d}E_L$ is the work performed on the ferromagnetic coil $\delta W = H_0 \mathrm{d}B_{V_L}$, plus the received heat $\delta Q = T_L \delta_e S$ where $\delta_e S$ is the variation of incoming entropy and δ denotes an inexact differential [28]:

$$\mathrm{d}E_L = H_0\, \mathrm{d}B_{V_L} + T_L \delta_e S. \tag{20}$$

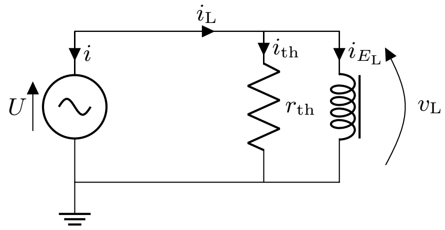

Figure 4: Voltage-controlled ferromagnetic coil with thermal dissipation.

The second principle of thermodynamics states that the internal heat $T_L \mathrm{d}S$ is the received heat plus the heat internally produced by irreversible phenomena $T_L \delta_i S$:

$$T_L \mathrm{d}S = T_L \delta_e S + T_L \delta_i S. \tag{21}$$

Replacing $T_L \delta_e S$ from Eq. (21) in Eq. (20) yields

$$\mathrm{d}G_{H_0} = \mathrm{d}E_L - T_L \mathrm{d}S - H_0 \mathrm{d}B_{V_L} = -T_L \delta_i S, \tag{22}$$

which is consistent with the assertion that the difference of energy is entirely and irreversibly dissipated as heat.
Now, let us denote H_L the observed effort law such as $H_0 = H_L(B_{V_L})$ (definition given in appendix A). Replacing H_0 with H_L, the entropy production rate $\delta_i S/\mathrm{d}t$ is obtained differentiating Eq. (22) with respect to B_{V_L} and multiplying with $\dot{B}_{V_L}$:

$$\frac{\delta_i S}{\mathrm{d}t} = \frac{1}{T_L}\left(H_L(B_{V_L}) - \frac{\partial E_L}{\partial B_{V_L}}(B_{V_L}, S)\right)\dot{B}_{V_L}. \tag{23}$$

To model the conversion between excess electro-magnetic power and thermal power, the ideal thermal exchanger r_{th} is introduced (Fig. 4) so that

$$i_{th} v_{th} = T_L \frac{\delta_i S}{\mathrm{d}t} \tag{24}$$

where v_{th} is the exchanger voltage and i_{th} its current. Introducing the function

$$P_{th} : \boldsymbol{x}_L \mapsto \left(H_L(B_{V_L}) - \frac{\partial E_L}{\partial B_{V_L}}(B_{V_L}, S)\right)\dot{B}_{V_L}, \tag{25}$$

equations (23-24) allow to model the dissipation in the PHS formalism:

$$\begin{aligned} &\boldsymbol{w} = [v_{th}, T_L]^\intercal \\ &z_{P_{th}(\boldsymbol{x}_L)}(\boldsymbol{w}) = [\frac{P_{th}(\boldsymbol{x}_L)}{v_{th}}, -\frac{P_{th}(\boldsymbol{x}_L)}{T_L}]^\intercal = [i_{th}, -\frac{\delta_i S}{\mathrm{d}t}]^\intercal. \end{aligned} \tag{26}$$

The passivity condition $P_{diss} \geq 0$ is fulfilled as $z(\boldsymbol{w})^\intercal \boldsymbol{w} = 0$. The complete PHS structure is given in section 4.4.

4. REFINED MODEL BASED ON MEASUREMENTS

4.1. Measurements and observations

As thermodynamically meaningful as the bi-stable model is, it does not capture the variety of phenomena contributing to hysteresis, as measurements on real ferromagnetic coils reveal. To conduct such measurements, a Fasel Red inductor (which can be found in Cry Baby wah-wah pedals [29] for instance) in series with

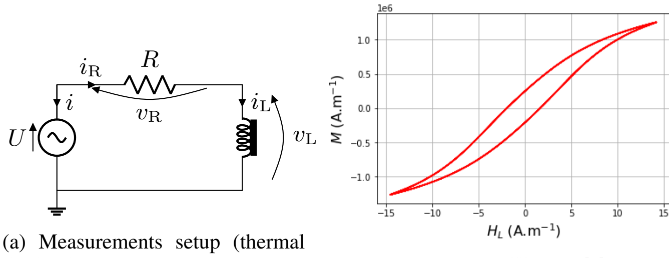

(a) Measurements setup (thermal dissipation not represented).

(b) Measured H_L and M.

Figure 5: Measurements setup and results.

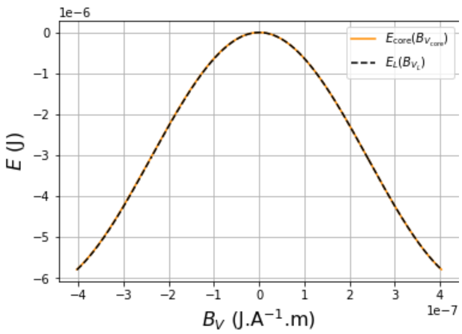

Figure 6: Core energy and coupled system equivalent energy computed with piecewise affine functions.

a resistance R is driven with a sinusoidal voltage source $U(t) = U_0 \sin(2\pi f_0 t)$ with f_0 = 8 Hz and U_0 = 0.35 V (Fig. 5a). The voltage v_L is measured and the current i_L is obtained through the relation $i_L = (U - v_L)/R$. The number of turns is roughly n = 150. The torus diameter d_1 and the torus section diameter d_2 are about respectively 10 mm and 3 mm, which yields $l = \pi d_1$ = 3.14 cm, $A = \pi(d_2/2)^2$ = 7.06 mm^2 and $V = Al$ = 22.2 mm^3. The magnetic field H_L and state B_{V_L} are then obtained using Eq. (17)-(18) and the relation $\Phi(t) = \int_0^t v_L(\tau)\,d\tau$. As the coil and the core share the same volume V, Eq. (11)-(13) yield the relation $B_{V_L} = \mu_0 V (H_L + M)$ from which M is obtained. These measurements (Fig. 5b) lead to two observations.

- First, M has an order of magnitude of 6, whereas H_L has an order of magnitude of 1, as expected for soft materials [17].
- Second, instead of the large jumps predicted by the bi-stable model, one observes a continuous progression, which calls for a model refinement to determine the entropy production rate law responsible for hysteresis.

4.2. Model reduction

According to measurements, for this inductor $B_{V_{core}} = \mu_0 M V \gg B_{V_{coil}} = \mu_0 H_L V$ and $E_{core} \gg E_{coil}$. The influence of the coil on the overall energy of the coupled component is negligible (Fig. 6) and we thus may use

$$E_L(B_{V_L}, S) \approx E_{core}(B_{V_L}, S). \tag{27}$$

The dynamics of the coupled system is therefore that of a driven core alone.

4.3. Entropy production rate law

In real ferromagnetic cores, domain structure and non-homogeneities [30] yield an energy function with not two but multiple local minima. Consequently, multiple Barkhausen jumps give the effort law the shape of a staircase. The Preisach model generates this effort law by computing a statistical mean on a collection of bi-stable systems such as the one presented in section 3, each one representing a domain. This averaging "damps" the large bi-stable jumps. Here, to obtain a similar result while remaining at a macroscopic level, the hysteresis loop is modeled using a cubic polynomial $P(\chi) = p_0 + p_1\chi + p_2\chi^2 + p_3\chi^3$ interpolating the effort $\frac{\partial E_L}{\partial B_{V_L}}$, and an additional friction term of the form $r_f \dot{B}_{V_L}$, $r_f \geq 0$, to account for thermal fluctuations [31] and eddy currents [32]. The coefficients of P are computed through

$$[p_0\ p_1\ p_2\ p_3]^\intercal = \boldsymbol{X}^{-1}\boldsymbol{Y}$$

where, given two interpolation data points χ_1 and χ_2, $\boldsymbol{X}$ and $\boldsymbol{Y}$ are defined as

$$\boldsymbol{X} = \begin{bmatrix} 1 & \cdots & \chi_1^3 \\ 1 & \cdots & \chi_2^3 \\ 0 & \cdots & 3\chi_1^2 \\ 0 & \cdots & 3\chi_2^2 \end{bmatrix}, \boldsymbol{Y} = \left[\frac{\partial E_L}{\partial B_{V_L}}(\chi_1) \dots \frac{\partial^2 E_L}{\partial B_{V_L}^2}(\chi_1) \dots\right]^\intercal.$$

The final hysteresis loop $\tilde{P}(B_{V_L})$ is thus defined by

$$\tilde{P}(B_{V_L}) = \delta_B P(\delta_B B_{V_L}) + r_f \dot{B}_{V_L}, \tag{28}$$

where $\delta_B = \mathrm{sign}(dB_{V_L})$, and the entropy production rate $\delta_i S/dt$ is:

$$\frac{\delta_i S}{dt} = \frac{1}{T_L}\left(\tilde{P}(B_{V_L}) - \frac{\partial E_L}{\partial B_{V_L}}(B_{V_L}, S)\right)\dot{B}_{V_L}, \tag{29}$$

which is the expression given in Eq. (23) where H_L has been replaced with $\tilde{P}$. For a given ferromagnetic coil, such a loop is accurate in a range from saturation approach to saturation and higher, provided that the data points are taken in that range. At lower fields though, a Rayleigh law would be more adequate [27].

4.4. Final model

Finally, Kirchhoff laws on the equivalent circuit shown on Fig. 4, together with Eq. (21), yield the PHS in Fig. 7 structured as in Eq. (1), in which E_L is given by Eq. (27)-(6), $\boldsymbol{w}$ and $z(\boldsymbol{w})$ are given by Eq. (26)-(29), $\boldsymbol{u} = [U, \delta_e S/dt]^\intercal$, $\boldsymbol{y} = [i, -T_{ext}]$.

4.5. Model identification with the Fasel inductor

The measurements are taken during an isothermal transformation, so that, replacing S from Eq. (3) in the magnetic field, one can use the expression

$$\frac{\partial E_L}{\partial B_{V_L}} = \frac{E_0}{B_{V_{L_s}}}\left(\frac{B_{V_L}}{B_{V_{L_s}}} - \tanh\left(\frac{B_{V_L}}{B_{V_{L_s}}\theta}\right)\right)$$

for identification. A least squares optimization between the Eq. (28) spline model and the measurements, i.e. solving $p = \mathrm{argmin}_p \| \left(H_L - \tilde{P}_p\left(B_{V_L}\right)\right)^2 \|^2$ with $p = [E_0, B_{V_{L_s}}, \theta, r_f]$ yields the parameters in Table 2. Figure 8 shows a good match between measurements and the estimated model.

		$\nabla E(\boldsymbol{x})$		$\boldsymbol{z}(\boldsymbol{w})$		$\boldsymbol{u}$	
		T_{L}	$\frac{\partial E_{\mathrm{L}}}{\partial B_{V_{\mathrm{L}}}}$	i_{th}	$-\frac{\delta_{\mathrm{i}} S}{\mathrm{d}t}$	U	$\frac{\delta_{\mathrm{e}} S}{\mathrm{d}t}$
$\dot{\boldsymbol{x}}$	$\dot{S}$	.	.	.	-1	.	1
	$\dot{B}_{V_{\mathrm{L}}}$	.	.	.	.	$\frac{l}{n}$	.
$\boldsymbol{w}$	v_{th}	.	.	.	.	1	.
	T_{L}	1	.	.	.	.	.
$\boldsymbol{y}$	i	.	$-\frac{l}{n}$	-1	.	.	.
	$-T_{\mathrm{ext}}$	-1	.	.	.	.	.

Figure 7: PHS of the voltage-controlled ferromagnetic coil with thermal dissipation. Dots in the interconnection matrix indicate zeros.

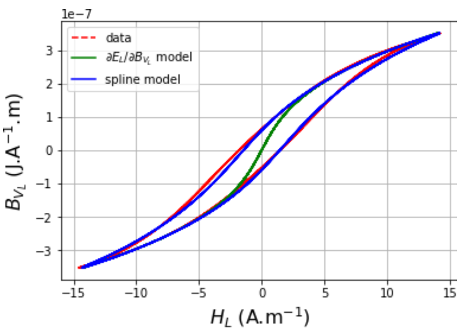

Figure 8: Measurements (red curve) and estimated spline model (blue curve).

5. APPLICATION TO A PASSIVE HIGH-PASS FILTER

5.1. Circuit modeling

The ferromagnetic coil model is used to simulate a high-pass filter (Fig. 9). The resistance R is linear of constitutive law $v_{\mathrm{R}}(i_{\mathrm{R}}) = Ri_{\mathrm{R}}$. Kirchhoff laws yield the PHS shown in Fig. 10.

5.2. Simulation

5.2.1. Discretization

The state vector $\boldsymbol{x}(t)$ is discretized to $\boldsymbol{x}[k] = \boldsymbol{x}(hk)$ where $h = 1/F_s$ is the sampling step, and we denote $\delta\boldsymbol{x}[k] = \boldsymbol{x}[k+1] - \boldsymbol{x}[k]$. To preserve the passivity of the PHS in discrete time and reduce the energy gradient sensitivity to the state indexing, we rely on the symmetric discrete energy gradient [10]. Denoting $n_{\boldsymbol{x}}$ the number of states, $\mathcal{P}(n_{\boldsymbol{x}})$ the set of all possible permutations on the $n_{\boldsymbol{x}}$ state indexes, $\boldsymbol{x}_\pi$ a permutation on the state indexes and E_π its corresponding energy, the symmetric discrete energy gradient $\overline{\nabla} E(\boldsymbol{x}, \delta\boldsymbol{x})$ is defined component-wise by:

$$\overline{\nabla} E(\boldsymbol{x}, \delta\boldsymbol{x})_i = \begin{cases} \dfrac{1}{n_{\boldsymbol{x}}!\,\delta x_i} \displaystyle\sum_{\pi \in \mathcal{P}(n_{\boldsymbol{x}})} \triangle_i(\boldsymbol{x}_\pi, \delta\boldsymbol{x}_\pi) & \delta x_i \neq 0 \\ \frac{\partial E}{\partial x_i} & \text{otherwise} \end{cases} \tag{30}$$

where $\triangle_i(\boldsymbol{x}, \delta\boldsymbol{x}) = E(\boldsymbol{x} + \overline{\delta\boldsymbol{x}}_i) - E(\boldsymbol{x} + \overline{\delta\boldsymbol{x}}_{i-1})$ and $\overline{\delta\boldsymbol{x}}_i = [\delta x_1, ..., \delta x_i, 0, ..., 0]^\intercal$. The discrete energy variation is obtained with the chain rule:

$$\frac{\delta E[k]}{h} = \overline{\nabla} E(\boldsymbol{x}[k], \delta\boldsymbol{x}[k])^\intercal \frac{\delta\boldsymbol{x}[k]}{h}. \tag{31}$$

The PHS of Fig. 10 is then approximated at sample k replacing $\dot{\boldsymbol{x}}$ with $\delta\boldsymbol{x}[k]/h$, $\nabla E(\boldsymbol{x})$ with $\overline{\nabla} E(\boldsymbol{x}[k], \delta\boldsymbol{x}[k])$, $\boldsymbol{w}$ with $\boldsymbol{w}[k]$, $\boldsymbol{u}$ with $\boldsymbol{u}[k]$ and $\boldsymbol{y}$ with $\boldsymbol{y}[k]$.

5.2.2. Newton-Raphson iteration

The interconnection matrix is decomposed as $\boldsymbol{J} = [\boldsymbol{J}_{\mathrm{stored}} \boldsymbol{J}_{\mathrm{diss}} \boldsymbol{J}_{\mathrm{ext}}]^\intercal$. We denote $\bar{\boldsymbol{e}}(\boldsymbol{x}[k], \delta\boldsymbol{x}[k]) = [\,\overline{\nabla} E(\boldsymbol{x}[k], \delta\boldsymbol{x}[k])\ \boldsymbol{z}(\boldsymbol{w}[k])\ \boldsymbol{u}[k]\,]^\intercal$, $\nu = \delta\boldsymbol{x}[k]$ and

$$F : \nu \mapsto \boldsymbol{J}_{\mathrm{stored}} \bar{\boldsymbol{e}}(\boldsymbol{x}[k], \nu) - \nu/h \tag{32}$$

At each sample k, $\delta\boldsymbol{x}[k]$ is solution of $F(\nu) = 0$. If $F'(\nu_i)$ is invertible and given an initial value ν_0 and a relative error ϵ_{r}, this solution can be computed iteratively with the update

$$\nu_{i+1} = \nu_i + \Delta_{\nu_i} \tag{33}$$

where $\Delta_{\nu_i} = -\left(F'(\nu_i)\right)^{-1} F(\nu_i)$, until $\|\Delta_{\nu_i}\|/\|\Delta_{\nu_0}\| \leq \epsilon_{\mathrm{r}}$. The state $\boldsymbol{x}[k+1]$ is then computed using $\boldsymbol{x}[k+1] = \boldsymbol{x}[k] + \delta\boldsymbol{x}[k]$.

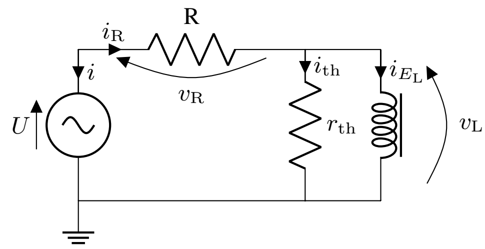

Figure 9: Passive high-pass filter.

		$\nabla E(\boldsymbol{x})$		$\boldsymbol{z}(\boldsymbol{w})$			$\boldsymbol{u}$	
		T_{L}	$\frac{\partial E_{\mathrm{L}}}{\partial B_{V_{\mathrm{L}}}}$	i_{th}	$-\frac{\delta_{\mathrm{i}} S}{\mathrm{d}t}$	v_{R}	U	$\frac{\delta_{\mathrm{e}} S}{\mathrm{d}t}$
$\dot{\boldsymbol{x}}$	$\dot{S}$	.	.	.	-1	.	.	1
	$\dot{B}_{V_{\mathrm{L}}}$	.	.	.	.	$-\frac{l}{n}$	$\frac{l}{n}$	.
$\boldsymbol{w}$	v_{th}	.	.	.	.	-1	1	.
	T_{L}	1	.	.	.	.	.	.
	i_{R}	.	$\frac{l}{n}$	1	.	.	.	.
$\boldsymbol{y}$	i	.	$-\frac{l}{n}$	-1	.	.	.	.
	$-T_{\mathrm{ext}}$	-1	.	.	.	.	.	.

Figure 10: PHS of the passive high-pass filter.

Estimated							
E_0	$B_{V_{\mathrm{L_s}}}$	θ	r_{f}	$\bar{p}_0$	$\bar{p}_1$	$\bar{p}_2$	$\bar{p}_3$
$2.43.10^{-5}$	$3.09.10^{-7}$	1.10	$6.07.10^{4}$	0	8.69	0	8.78
Given							
μ_0	k_{b}	n	V	$\bar{z}_1$	$\bar{z}_2$		
$4\pi.10^{-7}$	$1.38.10^{-23}$	150	$2.22.10^{-7}$	-1	1		

Table 2: Physical parameters of the model where $\bar{z}_i = z_i/B_{V_{\mathrm{L_s}}}$ and $\bar{p}_i = p_i B^i_{V_{\mathrm{L_s}}}$. The units are S.I. units given in Table 1.

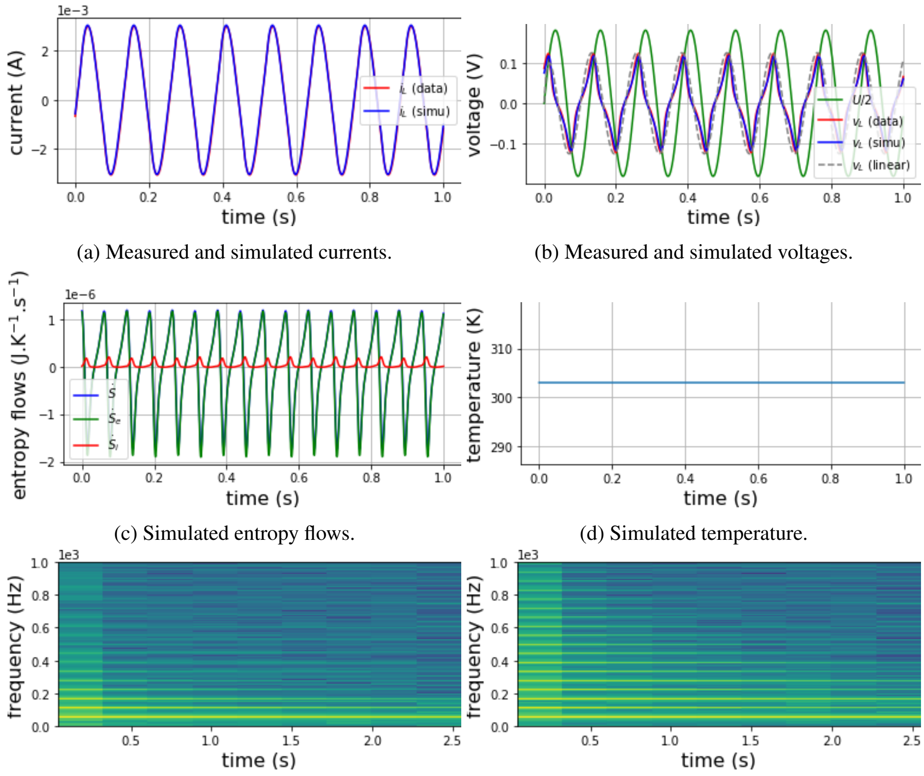

(a) Measured and simulated currents.

(b) Measured and simulated voltages.

(c) Simulated entropy flows.

(d) Simulated temperature.

(e) Bass sample spectrogram.

(f) Filtered bass sample spectrogram.

Figure 11: Simulation results.

Parameter	F_s	U_0	f_0	R
Value	96 kHz	0.35 V	8 Hz	100 Ω

Table 3: Simulation parameters.

5.2.3. *Simulation parameters*

The circuit is driven with a sinusoidal voltage whose parameters are given in Table 3, as well as with an instrumental bass sample. The ferromagnetic coil model parameters are those indicated in Table 2. The incoming entropy flow $\delta_e S/\mathrm{d}t$ is set so that the ferromagnetic coil temperature stays constant.

5.2.4. *Results and comparison to measurements*

The circuit is simulated with the non-linear coil model and a simple linear coil model ($i_L = \Phi_L/L$ with L = 840 mH) for comparison. Simulation results on Fig. 11a-11b show a good correspondence between the non-linear model and measurements. Fig. 11c-11d show that the produced entropy is always positive and that the coil temperature stays constant. Spectrograms of the bass sample is shown on Fig. 11e-11f. Sound results on the bass sample can be heard at `https://github.com/JNaj/dafx20-ferromag`.

6. CONCLUSION

In this paper, a physical and passive model of ferromagnetic coil has been developed. It is explicit and maintains a reduced number of variables and parameters.

First the core and the coil were treated separately, then their coupling, which determines both their electrical and thermal dynamics, was addressed. This lead to the building of an equivalent component, characterized by a well-established state, energy function, and entropy production rate law. A refined entropy production law based on measurements was then proposed.

As an application, this model was used to simulate a passive high-pass circuit. The simulations are in close agreement with measurements, though extensive measurements (a set of different frequencies, amplitudes, waveforms) would be required to validate the model on a broader scale.

Besides these complementary measurements, further work aims to assess real-time performances, and build a transformer model on the same principle by coupling two ferromagnetic coils.

7. REFERENCES

[1] David C Jiles and David L Atherton, "Theory of ferromagnetic hysteresis," *Journal of Magnetism and Magnetic Materials*, vol. 61, no. 1-2, pp. 48–60, 1986.

[2] David C Hamill, "Gyrator-capacitor modeling: a better way of understanding magnetic components," in *Proceedings*

of 1994 IEEE Applied Power Electronics Conference and Exposition-ASPEC'94. IEEE, 1994, pp. 326–332.

[3] Qianhong Chen, Ligang Xu, Xinbo Ruan, Siu Chung Wong, and C. K. Michael Tse, "Gyrator-capacitor simulation model of nonlinear magnetic core," *2009 Twenty-Fourth Annual IEEE Applied Power Electronics Conference and Exposition*, pp. 1740–1746, 2009.

[4] Giorgio Bertotti, "Dynamic generalization of the scalar preisach model of hysteresis," *IEEE Transactions on Magnetics*, vol. 28, no. 5, pp. 2599–2601, 1992.

[5] Sergey E Zirka, Yuriy I Moroz, Robert G Harrison, and Krzysztof Chwastek, "On physical aspects of the Jiles-Atherton hysteresis models," *Journal of Applied Physics*, vol. 112, no. 4, pp. 043916, 2012.

[6] Vincent François-Lavet, François Henrotte, Laurent Stainier, Ludovic Noels, and Christophe Geuzaine, "An energy-based variational model of ferromagnetic hysteresis for finite element computations," *Journal of Computational and Applied Mathematics*, vol. 246, pp. 243–250, 2013.

[7] M LoBue, Vittorio Basso, Carlo Paolo Sasso, and G Bertotti, "Entropy and entropy production in magnetic systems with hysteresis," *Journal of Applied Physics*, vol. 97, no. 10, pp. 10E513, 2005.

[8] B. M. Maschke, A. J. Van der Schaft, and P. Breedveld, "An intrinsic Hamiltonian formulation of network dynamics: Non-standard Poisson structures and gyrators," *Journal of the Franklin Institute*, pp. 923–966, 1992.

[9] Arjan van der Schaft, Dimitri Jeltsema, et al., "Port-Hamiltonian systems theory: An introductory overview," *Foundations and Trends® in Systems and Control*, vol. 1, no. 2-3, pp. 173–378, 2014.

[10] Antoine Falaize and Thomas Hélie, "Passive guaranteed simulation of analog audio circuits: A port-Hamiltonian approach," *Applied Sciences*, vol. 6, no. 10, pp. 273, 2016.

[11] Vincent Duindam, Alessandro Macchelli, Stefano Stramigioli, and Herman Bruyninckx, *Modeling and control of complex physical systems: the port-Hamiltonian approach*, Springer Science & Business Media, 2009.

[12] Ernst Ising, "Beitrag zur theorie des ferromagnetismus," *Zeitschrift für Physik*, vol. 31, no. 1, pp. 253–258, 1925.

[13] Gordon F Newell and Elliott W Montroll, "On the theory of the Ising model of ferromagnetism," *Reviews of Modern Physics*, vol. 25, no. 2, pp. 353, 1953.

[14] Jozef Strecka and Michal Jascur, "A brief account of the Ising and Ising-like models: Mean-field, effective-field and exact results," *arXiv preprint arXiv:1511.03031*, 2015.

[15] Franz Utermohlen, "Mean field theory solution of the Ising model," `https://cpb-us-w2.wpmucdn.com/u.osu.edu/dist/3/67057/files/2018/09/Ising_model_MFT-25b1klj.pdf`.

[16] Louis Néel, "Magnetism and local molecular field," *Science*, vol. 174, no. 4013, pp. 985–992, 1971.

[17] Colonel Wm T McLyman, *Transformer and inductor design handbook*, CRC press, 2016.

[18] Barry M McCoy and Tai Tsun Wu, *The two-dimensional Ising model*, Courier Corporation, 2014.

[19] R Stuart and W Marshall, "Direct exchange in ferromagnets," *Physical Review*, vol. 120, no. 2, pp. 353, 1960.

[20] Michael Ellis Fisher, "Lattice statistics in a magnetic field, I. A two-dimensional super-exchange antiferromagnet," *Proceedings of the Royal Society of London. Series A. Mathematical and Physical Sciences*, vol. 254, no. 1276, pp. 66–85, 1960.

[21] Patric W Anderson and H Hasegawa, "Considerations on double exchange," *Physical Review*, vol. 100, no. 2, pp. 675, 1955.

[22] GS Rushbrooke and P Jo Wood, "On the Curie points and high temperature susceptibilities of Heisenberg model ferromagnetics," *Molecular Physics*, vol. 1, no. 3, pp. 257–283, 1958.

[23] Edwin T Jaynes, "On the rationale of maximum-entropy methods," *Proceedings of the IEEE*, vol. 70, no. 9, pp. 939–952, 1982.

[24] Daniel J Amit and Yosef Verbin, *Statistical physics: An introductory course*, World Scientific Publishing Company, 1999.

[25] AJ Van der Schaft, "Port-Hamiltonian differential-algebraic systems," in *Surveys in Differential-Algebraic Equations I*, pp. 173–226. Springer, 2013.

[26] Judy Najnudel, Thomas Hélie, and David Roze, "Simulation of the ondes Martenot ribbon-controlled oscillator using energy-balanced modeling of nonlinear time-varying electronic components," *Journal of the Audio Engineering Society*, vol. 67, no. 12, pp. 961–971, 2019.

[27] Giorgio Bertotti, *Hysteresis in magnetism: for physicists, materials scientists, and engineers*, Academic press, 1998.

[28] Peter T Landsberg, *Thermodynamics and statistical mechanics*, Courier Corporation, 2014.

[29] Antoine Falaize-Skrzek and Thomas Hélie, "Simulation of an analog circuit of a wah pedal: a port-Hamiltonian approach," in *Audio Engineering Society Convention 135*. Audio Engineering Society, 2013.

[30] Charles Kittel, "Physical theory of ferromagnetic domains," *Reviews of modern Physics*, vol. 21, no. 4, pp. 541, 1949.

[31] W Brown, "Thermal fluctuation of fine ferromagnetic particles," *IEEE Transactions on Magnetics*, vol. 15, no. 5, pp. 1196–1208, 1979.

[32] CD Graham Jr, "Physical origin of losses in conducting ferromagnetic materials," *Journal of Applied Physics*, vol. 53, no. 11, pp. 8276–8280, 1982.

A. DEFINITION OF THE BI-STABLE MODEL OBSERVED EFFORT LAW H_{L}

Denoting $B_{V_{\mathrm{L}_0}} \geq 0$ such as $\frac{\partial^2 E_{\mathrm{L}}}{\partial B_{V_{\mathrm{L}}}^2}(B_{V_{\mathrm{L}_0}}) = 0$ (Fig. 3b, green cross), and $\tilde{B}_{V_{\mathrm{L}_0}} \leq 0$ such as $\frac{\partial E_{\mathrm{L}}}{\partial B_{V_{\mathrm{L}}}}(\tilde{B}_{V_{\mathrm{L}_0}}) = H_{\mathrm{coerc}}$ (Fig. 3b, green plus), one can define H_{L} as:

$$H_{\mathrm{L}}(B_{V_{\mathrm{L}}}) = \begin{cases} -\mathrm{sign}(\mathrm{d}B_{V_{\mathrm{L}}}) H_{\mathrm{coerc}} & B_{V_{\mathrm{L}}} \in [B_{V_{\mathrm{L}\inf}}, B_{V_{\mathrm{L}\sup}}] \\ \frac{\partial E_{\mathrm{L}}}{\partial B_{V_{\mathrm{L}}}} & \text{otherwise} \end{cases},$$

where $[B_{V_{\mathrm{L}\inf}}, B_{V_{\mathrm{L}\sup}}] = [\tilde{B}_{V_{\mathrm{L}_0}}, B_{V_{\mathrm{L}_0}}]$ if $\mathrm{d}B_{V_{\mathrm{L}}} \leq 0$ and $[-B_{V_{\mathrm{L}_0}}, -\tilde{B}_{V_{\mathrm{L}_0}}]$ otherwise.